IEEE Access
Multidisciplinary | Rapid Review | Open Access Journal

Received August 8, 2019, accepted August 25, 2019, date of publication August 29, 2019, date of current version December 23, 2019.

Digital Object Identifier 10.1109/ACCESS.2019.2938270

Free-Electron-Driven Multi-Frequency Terahertz Radiation on a Super-Grating Structure

JUAN-FENG ZHU, CHAO-HAI DU, (Senior Member, IEEE), FAN-HONG LI, LU-YAO BAO, AND PU-KUN LIU, (Senior Member, IEEE)

State Key Laboratory of Advanced Optical Communication Systems and Networks, Department of Electronics, Peking University, Beijing 100871, China

Corresponding author: Chao-Hai Du (duchaohai@pku.edu.cn)

This work was supported in part by the National Natural Science Foundation of China under Contract 61531002, NSAF U1830201, and 61861130367, and in part by the Newton Advanced Fellowship from the Royal Society, U.K., under Contract NAF/R1/180121.

ABSTRACT A free-electron-driven multi-frequency terahertz (THz) radiation based on a super-grating structure is elucidated in this paper. The super-grating, i.e., periodically depth-modulated metallic grating, has a peculiar dispersion characteristic, similar to the energy bands in a crystal due to the Brillouin zone folding effect. The multi-frequency radiation is stimulated in several directions with the excitation of a free electron as the synchronization points are in the radiative region. The radiation frequency can be independently tuned by the groove depths of the super-grating. The number of frequencies is tailored by the modulated period. Additionally, the multi-frequency THz radiation exhibits a frequency-locked effect during the energy variation of the free electron. Moreover, the radiation field intensity shows a significant enhancement compared with that of a conventional Smith-Purcell radiation. The work is promising for developing efficient on-chip THz radiation sources and boosts advanced THz applications such as communications, multi-frequency imaging, and beam diagnostics, etc.

INDEX TERMS Terahertz radiation, spoof surface plasmon, vacuum electronics, multi-frequency radiation.

I. INTRODUCTION

Terahertz (THz) sources play a key role in promoting the development of THz technologies [1]–[3]. Compared with other THz sources such as the optical devices [4], solid state electron devices [5], vacuum electronic devices (VEDs) [6]–[9] are excellent candidates for generating high power THz radiation. Recently, the exploitation of spoof surface plasmon (SSP) has brought new possibilities to the VEDs for its intriguing characteristics such as the local resonant effect, strong near-field confinement and so on [10]–[12]. Since then, THz radiation sources based on the beam-wave interaction between the free electron and SSP wave have been fully investigated. For example, the beam-SSP interactions in single grating, double grating, gradient grating and crystal-like structures have been extensively studied to generate a coherent THz radiation [13]–[16].

Despite the coherent THz radiation based on the SSP wave can be obtained from the beam-SSP interaction, the SSP is confined at the surface of grating as its wavenumber is considerably larger than that of propagation wave [13], [14]. It is crucial to convert the SSP wave into fast wave, and several approaches are aimed at overcoming this obstacle. For instance, the gradient waveguide and the meta-surface structure could achieve it [17], [18]. However, it is challenging to achieve an effective conversion in an on-chip system because of the limitation of manufacturing difficulties, high-power capacity and electron bombardment. Although the SSP can be diffracted into a spatial directional radiation at the end of a graded grating, the radiation direction is fixed [19]. For various advanced THz applications, such as communications, it is imperative to explore an effective free-electron-driven on-chip THz radiation source. Whereas, the Smith-Purcell radiation (SPR) has been expected as a promising candidate [20]–[22]. The SPR-like spatial radiation are investigated in a high-Q Fano grating, and the radiation characteristics strongly depends on the electromagnetic resonance in the structure [23]. Despite the spatial radiation can be achieved, the multi-frequency radiation has not been extensively investigated.

In this paper, a free-electron-driven multi-frequency THz radiation is achieved based on a super-grating. The super-grating, i.e., periodically depth-modulated metallic grating, has a peculiar dispersion characteristic, similar to the energy

The associate editor coordinating the review of this article and approving it for publication was Yue Zhang.

bands in a crystal due to the Brillouin zone folding effect. In this manner, part of the dispersion curve is folded into the radiative region. When the free electron closely moves to the super-grating, the multi-frequency THz radiation is generated in several specific directions consequently. The radiation frequencies are independently tuned by the modulated depth of super-grating, and the number of radiation frequencies is tailored by the modulated period. The radiation direction is determined by the energy of the free electron and radiation frequency. As the super-grating can be equivalent to a series of SSP cavities, the multi-frequency THz radiation exhibits a frequency-locked effect during the dynamic voltage tuning of free electron owing to the resonance characteristic in these cavities. Additionally, the radiation intensity is manipulated by the coupling between the different cavities. Moreover, the electric field intensity of the multi-frequency THz radiation shows an enhancement about 6 times in comparison with that of the conventional SPR. These intriguing characteristics cannot be expected from the conventional SPR devices. Furthermore, the multi-frequency radiation provides a new way for developing on-chip THz radiation sources and holds promises in various advanced THz applications.

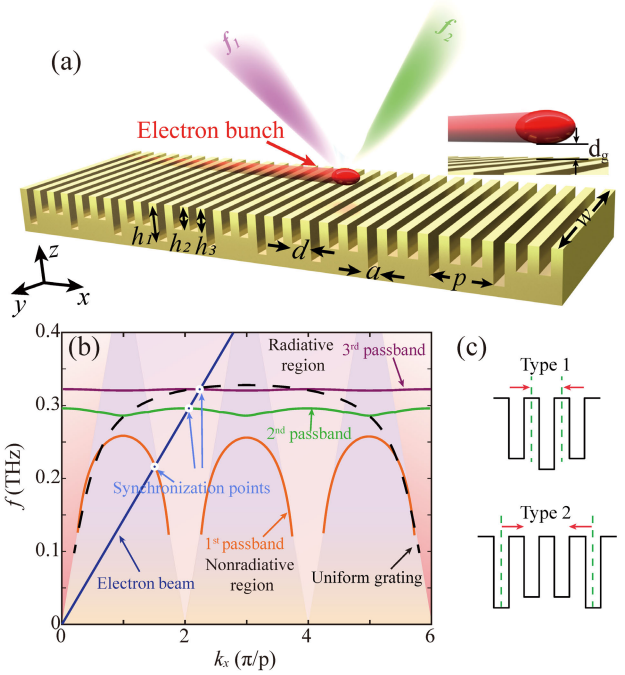

FIGURE 1. (a) The schematic model of the multi-frequency THz radiation. The free electron passes over the super-grating and gives rise to the multi-frequency radiation in several specific directions. (b) The dispersion curve of the super-grating is shown in solid lines and the dispersion curve of the uniform grating with depth $h = 0.2$ mm is shown as the black dashed line. (c) Two different types of cavities in a period of the super-grating.

II. MODEL PRESENTATION

The schematic diagram of multi-frequency THz radiation based on a super-grating is shown in Fig. 1(a). The super-grating has a uniform period d, and width a. The modulation period is p, and the width of the grating is w. In a super-cell, the groove depths are modulated periodically as h_1, h_2 and h_3, respectively. The operation voltage of the electron bunch is U. The distance between the free electron and the grating surface is d_g. As a form of Fano metamaterial, the super-grating has been widely studied in the past decades, and its high-Q property is promising for various applications in VEDs [23], [24]. However, the multi-frequency radiation characteristic has not been explored. In order to make a clear investigation about the physical mechanism, the dispersion characteristic is studied. We assume the width of this grating is infinite in y direction and only focus on the SSP mode in the x–z plane. The dispersion equation $|M| = 0$ is derived based on the mode matching method with perfect electric conductor boundary conditions [25], [26]. The matrix M is depicted in (1) (see appendix A).

$$M\left(k', k\right) = S_{k'-k} - \delta_{k'k} T_k \tag{1a}$$

$$S_{k'-k} = \sum_{n=-\infty}^{\infty} j \frac{k_0}{k_{zn}} \left(\frac{a}{p}\right) Sa^2\left(\frac{k_{xn} a}{2}\right) e^{jk_{xn}(k-k')d} \tag{1b}$$

$$T_k = cot\left(k_0 h_k\right) e^{-jk_{x0}kd} \tag{1c}$$

where $k = 1, 2, 3$, $k' = 1, 2, 3$, h_k is the depth in the k-th groove. $k_0 = 2\pi f/c$ is the wave number in the free space. c is the light speed. $k_{xn} = k_{x0} + 2\pi n/p$ is the longitudinal wave vector of the n-th harmonic mode, and $k_{xn}^2 + k_{zn}^2 = k_0^2$. $\delta_{k'k}$ is the Kronecker function. $Sa\left(x\right) = sinx/x$. Additionally, the dispersion equation of the free electron can be expressed in (2)

$$\omega = v_e k_x \tag{2a}$$

$$v_e = c\sqrt{1 - 1/\left(1 + \frac{eU}{m_0 c^2}\right)^2} \tag{2b}$$

where v_e is the velocity of the free electron, e is the electron charge, m_0 is the electron mass, U is the operation voltage. In this work, we use the following parameters: $d = 0.1$ mm, $a = 0.05$ mm, $p = 3d$, $d_1 = 0.25$ mm, $h_2 = h_3 = 0.2$ mm, $d_g = 0.01$ mm, $w = 0.5$ mm, and $U = 36$ kV.

The dispersion curves of super-grating and uniform grating are presented in Fig. 1(b). Though the geometric structures of both super-gratings and uniform ones are similar, the physical characteristics are significantly distinct. The dispersion curve of the super-grating splits into a series of passbands, which resembles the energy bands in a crystal. There are three passbands that are marked with the 1st passband, 2nd passband and so on. As shown in the Fig. 1(b), the extra radiative region emerges in the nonradiative region in the Brillouin zone of the uniform grating, which is caused by the Brillouin zone folding effect [27]. Furthermore, the appearance of radiative region implies the radiative characteristic of this system. The dispersion curves in 2nd and 3rd passbands tend to be straight and the frequency ranges of these passbands are narrow. This peculiar characteristic can be explained by the cavity resonance effect. In general, the uniform grating is considered as a SSP waveguide. If the depth of grating is modulated

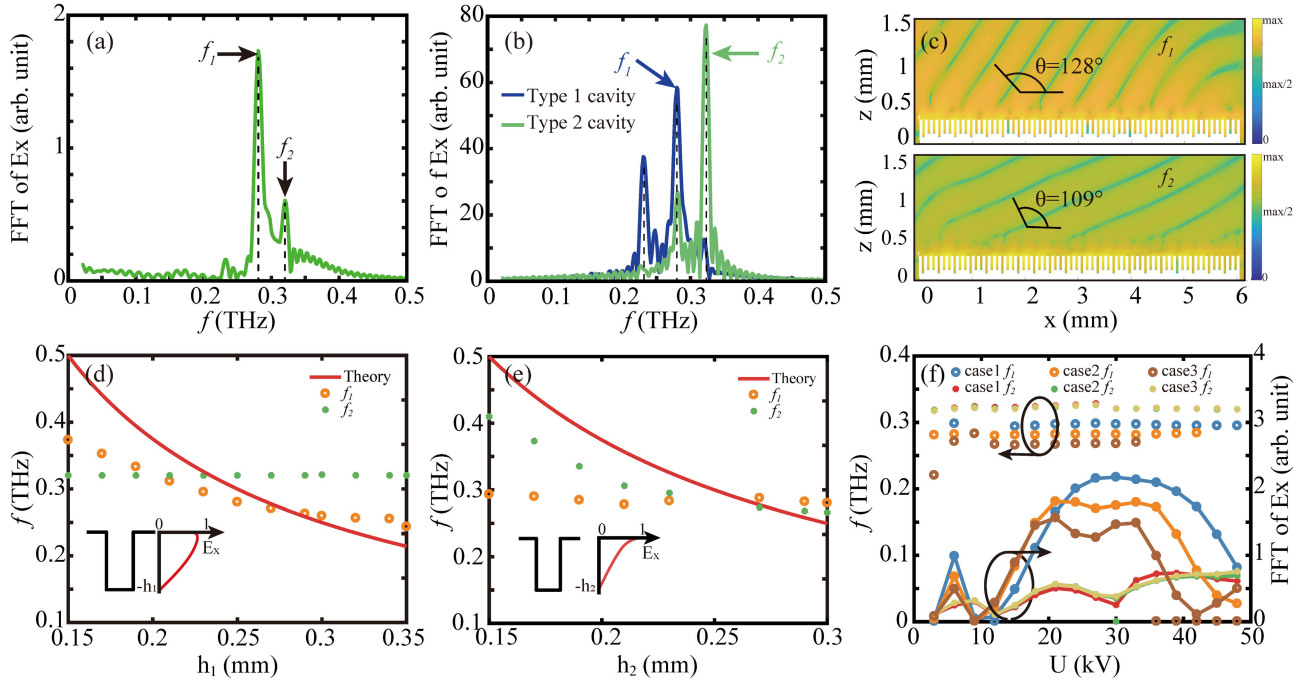

FIGURE 2. Simulation results of the multi-frequency THz radiation. (a) The FFT spectrum in the far field. (b) The FFT spectra in the type 1 cavity and the type 2 cavity. (c) The contour maps of the Ex component at radiation frequencies. (d)-(e). Variations of the radiation frequencies with the groove depth in different type cavities. The radiation frequency predicted by the resonant condition are shown in red solid lines, and obtained from the PIC solver are shown in dots and circles. (d) The radiation frequencies change with the depth in type 1 cavity. The groove depth in type 2 cavity is set: $h_2 = 0.2$ mm. Inset: The distributions of the E_x component in the z direction for the type 1 cavity. (e) The radiation frequencies change with the depth in type 2 cavity. The groove depth in type 1 cavity is set: $h_1 = 0.25$ mm. Inset: The distributions of the E_x component in the z direction for the type 2 cavity. (f) The frequency spectrum versus the energy of the free electron. There are three cases with $h_2 = 0.2$ mm, case 1: $h_1 = 0.23$ mm, case 2: $h_1 = 0.25$ mm, case 3: $h_1 = 0.27$ mm.

periodically, the uniformity of the SSP waveguide is broken and results in reflections in this system consequently. In this way, there are a series of reflectors in the super-grating and adjacent reflectors form a SSP cavity. As shown in Fig. 1(c), there are two types of SSP cavities in a super-cell of the super-grating named type 1, type 2. The dispersion curves in the 2nd and 3rd passbands represent the resonant modes in these cavities. Moreover, this resonant characteristic implies the frequency-locked effect, and may be applied for developing a stable THz radiation source.

III. MULTI-FREQUENCY TERAHERTZ RADIATION

As shown in the Fig. 1(b), there are two synchronization points between the electron beam line and the dispersion curve of the super-grating in the radiative region. The multi-frequency THz radiation operating at these synchronization frequencies will be stimulated with the electron excitation. The theoretical analysis is verified using the particle-in-cell (PIC) solver in the commercial software CST studio and the single electron particle model is utilized to stimulate the multi-frequency THz radiation. A 50-μm-wide beam bunch with Gaussian charge distribution moves above the super-grating. The charge of the electron bunch is 1.6e-19 C, and the acceleration energy of the electron beam is the operation voltage [28]. The simulation results are depicted in Fig. 2. The frequency spectra at far field, type 1 cavity, type 2 cavity are presented in Figs. 2(a) and 2(b). As there are three synchronization points, and two of them are in radiative region, there are two peaks in far field and three peaks in type 1 cavity, type 2 cavity. The frequency peaks at far field are marked as $f_1 = 0.28$ THz, $f_2 = 0.32$ THz, and the corresponding electric profiles are shown in Fig. 2(c).

The relation between the radiation direction and frequency can be obtained according to the wave vector matching method as shown in (3) (see appendix B), which is identical to the SPR relation [20], [21].

$$\frac{c}{f} = \frac{L}{|n|}\left(\frac{v_e}{c} - cos\theta\right) \tag{3}$$

where θ is the radiation angle with respect to the propagation direction of the free electron, L is the diffraction period. The integer n refers to the n-th harmonic wave. For the super-grating, $L = p$. The electric field profiles at frequencies f_1 and f_2 are presented in Fig. 2(c) and the radiation angles are 128°, 109°, respectively, which are well agreed with the calculated results according to (3) ($n = -1$, $v_e = 0.35\ c$). Since the single electron bunch model is employed in the PIC simulation, the radiation spectrum inevitably extends to a certain frequency bandwidth [29].

The physical process of stimulating the multi-frequency THz radiation is analyzed in this paragraph. The SSP is initially excited by the free electron along the grating and

then trapped in different types of cavities. The diffraction occurs owing to the mismatch in wavenumber between the propagating SSP mode and the trapped modes. The resonant frequencies of the type 1 cavity, type 2 cavity are f_1, f_2 respectively. Type 1 cavities and type 2 cavities are arranged alternately in the super-grating. The length of the type 2 cavity is sufficiently long, as a result of which the coupling between the adjacent type 1 cavities is weak. Whereas, the length of the type 1 is not sufficiently long so that the coupling between the adjacent type 2 cavities is stronger than that between the adjacent type 1 cavities. In this manner, the SSP waves in both type 1 and 2 cavities will radiate into the free space, and the electric intensity at f_1 is higher than that at f_2. Following the above analysis, the multi-frequency radiation mechanism based on a super-grating can be uncovered as below. When the free electron skims along the super-grating, which is equivalent to a series of cavities, the resonant mode in each cavity is excited one by one. Owing to the suppressed coupling between adjacent same type cavities, these resonant modes independently radiate into free space, behaving like an antenna array.

IV. DISSCUSSION

Given the above description, the radiation frequencies are determined by the synchronization frequencies, which correspond to the resonant frequencies in the super-grating. The resonant condition can be approximately depicted as:

$$\lambda = \frac{h}{1/2 + m/4} \tag{4}$$

where m is an integer, indicating the mode number. h is the depth of the groove [29]. In this study, the fundamental mode (m = 0) is considered. The radiation frequencies with different depths of the grooves are presented in Figs. 2(d) and 2(e). The radiation frequency predicted by the resonant condition are shown in red solid lines, and obtained from the PIC solver are presented in dots and circles. With h_1 increasing, the radiation frequency f_1 decreases whereas f_2 keeps steady. With h_2 increasing, the radiation frequency f_2 decreases, while f_1 holds steady. The variation of the radiation frequencies with different groove depths indicates that both f_1 and f_2 are tuned by altering the depths independently in type 1 and 2 cavities, which provides a convenient way to manipulate the radiation frequency. However, as the type 1 and 2 cavities are open resonant cavities, the field distribution at the opening of the cavities is so complex that the resonant equation cannot precisely describe the resonant frequency. Despite the difference between the simulation and theoretical approximation, the tendency of the radiation frequencies obtained from the PIC simulation are mostly consistent with the theoretical analysis according to the resonant condition illustrated by (4).

The variations of the radiation frequencies with different beam energy are presented in Fig. 2(f). There are three different sets of parameters with $h_2 = 0.2$ mm, case 1: $h_1 = 0.23$ mm, case 2: $h_1 = 0.25$ mm, case 3: $h_1 = 0.27$ mm. As shown in the Fig. 2(f), the radiation frequencies have little fluctuation with the voltage varying in different cases, indicating the frequency-locked characteristic of the multi-frequency THz radiation. The stable radiation frequency arises from the resonance in super-grating. Besides, the field intensity at f_1 is higher than that at f_2, which well matches with the previous description. More, since the synchronization point shifts into the nonradiative region when the energy of the free electron is high (for example, at U = 48 kV), the multi-frequency radiation is absent, and the spectrum intensity drastically decreases consequently.

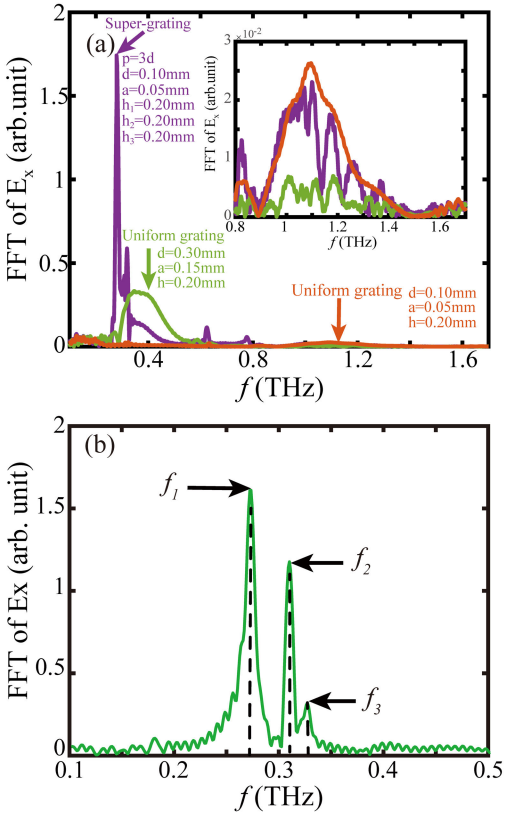

FIGURE 3. (a) Comparison with the multi-frequency SPR excited in the super-grating and the ordinary SPR excited in the uniform grating. Inset: In the frequency region of the ordinary SPR, the intensity of the multi-frequency SPR is in good agreement with that of the ordinary SPR. (b) Radiation frequency spectrum with the modulated period *4d*. There are three radiation frequencies.

In a uniform grating, the SSP is confined at the surface and only the conventional SPR radiates into the space. For the uniform grating, the lowest radiation frequency range is (0.79 - 1.66 THz) according to (3) ($L = d = 0.1$ mm, $n = -1$, $v_e = 0.357c$). Compared with the FFT frequency spectrum from a super-grating, the radiation peak near 0.3 THz is absent in the uniform grating as a result. In order to shift the conventional SPR in the same frequency range with the multi-frequency THz radiation, the parameters of the uniform grating are changed as $d = 0.3$ mm, $a = 0.15$ mm, and $h = 0.2$ mm. The simulation result is shown as the green line in Fig. 3(a). The maximum spectrum intensity of

the multi-frequency radiation is about 6 times higher than that of the conventional SPR from the uniform grating at the frequency range near 0.3 THz, indicating that the multi-frequency THz radiation is promising for developing a compact and efficient radiation source. Furthermore, if the depth modulated period p increases, the multi-frequency THz radiation effect becomes apparent. The stimulation result with $p = 4d$ ($d = 0.1$ mm, $a = 0.05$ mm, $h_1 = 0.25$ mm, $h_2 = h_3 = h_4 = 0.2$ mm) is presented in Fig. 3(b), and there are three radiation peaks: $f_1 = 0.27$ THz, $f_2 = 0.308$ THz and $f_3 = 0.325$ THz. Generally, when $p = md$, the Brillouin zone ($-\pi$/d, π/d) of the uniform grating is divided into m new Brillouin zones. There are $m-1$ forbidden bands and m passbands. Since the lowest passband is confined at the nonradiative region, there are at most $m-1$ synchronization points in the radiative region, corresponding to $m-1$ radiation frequencies. The dominant radiation frequency is determined by the resonant frequency of type 1 cavity and is tuned by the groove depth h_1. The dispersion curves in high order passbands will be narrow, and the frequency-locked effect will be significant consequently. In fact, other kinds of resonators can also be used instead of the rectangular grating to generate the multi-frequency radiation based on the mechanism rendered in this paper. Additionally, the simplest depth modulated way of a uniform grating is considered here.

V. CONCLUSION

A multi-frequency THz radiation mechanism based on a super-grating structure is demonstrated in this paper. The extraordinary dispersion characteristic due to the Brillouin zone folding effect is analyzed, and new radiative region appears in the nonradiative region of the uniform grating. The super-grating is considered as a series of cavities. When the free electron bunch moves over these cavities, the SSP is initially excited and trapped in these cavities. The weak coupling between the adjacent type cavities gives rise to this unconventional multi-frequency THz radiation in specific directions. The radiation frequencies are determined by the synchronization frequencies between the electron beam lines and dispersion curves, i.e., resonant frequencies in different cavities, and are independently tuned by the groove depths in these cavities. Furthermore, the radiation possesses frequency-locked characteristic with the energy variation of the free electron. Compared with the SPR from a uniform grating, the intensity is significantly enhanced. The multi-frequency THz radiation demonstrated in this paper provides a good paradigm for developing on-chip THz radiation sources, and has potential THz applications such as communications, imaging.

APPENDIX A
DERIVATION OF THE DISPERSION EQUATION

Considering the SSP mode is a quasi -2D electromagnetic excitation, and the SSP mode in x-z plane is analyzed here. The schema of a super-grating model is shown in Fig. 4. The width of the groove is a, and the local period of the groove

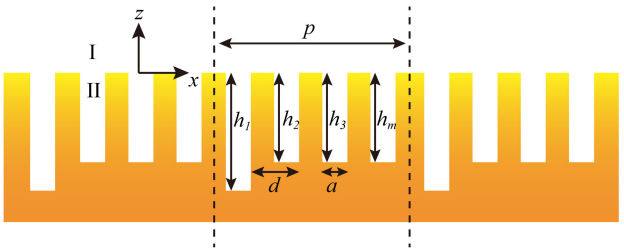

FIGURE 4. The model of the super-grating.

is d. There are m grooves in a supercell, and the depths of these grooves are $h_1, h_2, \ldots h_m$, respectively. The length of a supercell is p.

The space is divided into two regions as shown in Fig. 4. In the THz range, the metal behaves like a perfect electric conductor, and the field expressions in these regions are illustrated as (5-6).

In region I:

$$H_y^{\mathrm{I}}(x,z) = \sum_{n=-\infty}^{+\infty} R_n e^{-j(k_{xn}x+k_{zn}z)} \tag{5a}$$

$$E_x^{\mathrm{I}}(x,z) = \frac{1}{j\omega\varepsilon_0}\frac{\partial H_y^I}{\partial z} = \sum_{n=-\infty}^{+\infty} \frac{k_{zn}}{\omega\varepsilon_0} R_n \mathrm{e}^{-j(k_{xn}x+k_{zn}z)} \tag{5b}$$

where R_n is the coefficients of n-th harmonic wave, $k_{xn} = k_{x0} + 2\pi/p$ is the longitudinal wave vector of n-th harmonic wave. k_{x0} is the wave vector of 0-th harmonic wave. $k_{zn} = \sqrt{k_0^2 - k_{xn}^2}$, $k_0 = 2\pi f/c$ is the wave number in the free space.

In region II, since the width is much less than the wavelength in space ($a \ll \lambda$), the mode we need to consider is the TEM mode propagating in the $\pm z$ directions. The phase shift along x must be considered as a discontinuous function $\mathrm{e}^{jk_{x0}kd}$ in the k-th groove.

We have

$$H_y^{\mathrm{II}} = -j\frac{\omega\varepsilon_0}{k_0}\sum_{k=1}^{m} B_k M_k(x)\frac{\cos[k_0(z+h_k)]}{\sin(k_0 h_k)} e^{-jk_{x0}kd} \tag{6a}$$

$$E_x^{\mathrm{II}} = \sum_{k=1}^{m} B_k M_k(x)\frac{\sin[k_0(z+h_k)]}{\sin(k_0 h_{\mathrm{k}})} e^{-jk_{x0}kd} \tag{6b}$$

where $M_k(x) = rect[\frac{x-\left(k-\frac{m+1}{2}\right)d}{a}]$ is the field form in the k-th groove, rect( ) is the rectangular function, and the amplitude coefficient B_k is unknown variable which could be determined by the boundary conditions.

At the $z=0$ interface,

$$E_x^{\mathrm{I}}(x,0) = \sum_{n=-\infty}^{+\infty} \frac{k_{zn}}{\omega\varepsilon_0} R_n \mathrm{e}^{-jk_{xn}x} \tag{7a}$$

$$E_x^{\mathrm{II}}(x,0) = \sum_{k=1}^{m} B_k M_k(x) e^{-jk_{x0}kd} \tag{7b}$$

$$H_y^{\mathrm{I}}(x,0) = \sum_{n=-\infty}^{+\infty} R_n e^{-jk_{xn}x} \tag{8a}$$

$$H_y^{\mathrm{II}}(x,0) = -j\frac{\omega\varepsilon_0}{k_0}\sum_{k=1}^{m} B_k M_k(x)\cot(k_0 h_k) e^{-jk_{x0}kd} \tag{8b}$$

According to the electric boundary condition, it yields,

$$\sum_{n=-\infty}^{+\infty} \frac{k_{zn}}{\omega\varepsilon_0} R_n \mathrm{e}^{-jk_{xn}x} = \sum_{k=1}^{m} B_k M_k(x)\, e^{-jk_{x0}kd} \tag{9}$$

Considering the orthogonality of different diffraction orders, we multiply (9) by $\mathrm{e}^{jk_{xn}x}$ and then integrate over $(-p/2, p/2)$. It yields,

$$\frac{k_{zn}}{\omega\varepsilon_0} pR_n = aSinc(\frac{k_{xn}a}{2}) \sum_{k=1}^{m} B_k M_k(x)\, e^{jk_{xn}\left(k-\frac{m+1}{2}\right)d} \times e^{-jk_{x0}kd} \tag{10}$$

Thus, R_n can be expressed in terms of B_k,

$$R_n = \frac{\omega\varepsilon_0}{k_{zn}}(\frac{a}{p}) Sinc\left(\frac{k_{xn}a}{2}\right) \sum_{k=1}^{m} B_k M_k(x)\, e^{jk_{xn}\left(k-\frac{m+1}{2}\right)d} e^{-jk_{x0}kd} \tag{11}$$

The exact matching condition for the magnetic field H_y at the boundary $z = 0$ cannot be satisfied simultaneously, for it is trial function but not actual fields in the gap region. The magnetic field H_y can only be matched approximately by applying the average matching condition, i.e. the integrals of the field H_y along the surface (z = 0) are equal. Given the orthogonality of rectangular function, we multiply (8a) (8b) by $M_{k'}(x)$, then integrate over $(-p/2,p/2)$ respectively. It yields,

$$\sum_{n=-\infty}^{\infty} R_n Sa\left(\frac{k_{xn}a}{2}\right) e^{-jk_{xn}\left(k'-\frac{m+1}{2}\right)d} = -j\frac{\omega\varepsilon_0}{k_0} B_{k'} M_{k'}(x)\, cot(k_0 h_{k'})\, e^{-jk_{x0}k'd} \tag{12}$$

where $k' = 1, 2, 3, \ldots m$.

Substituting (11) into (12), it yields,

$$\sum_{n=-\infty}^{\infty} \frac{\omega\varepsilon_0}{k_{zn}}(\frac{a}{p}) Sa\left(\frac{k_{xn}a}{2}\right) \sum_{k=1}^{m} B_k M_k(x) e^{jk_{xn}\left(k-\frac{m+1}{2}\right)d} \times e^{-jk_{x0}kd} - j\frac{\omega\varepsilon_0}{k_0} B_{k'} M_{k'}(x)\, cot(k_0 h_{k'})\, e^{-jk_{x0}k'd} \tag{13}$$

Then simplify and we can get,

$$\sum_{n=-\infty}^{\infty} \sum_{k=1}^{m} B_k M_k(x)\, j\frac{k_0}{k_{zn}} \left(\frac{a}{p}\right) Sa^2\left(\frac{k_{xn}a}{2}\right) \times e^{jk_{xn}(k-k')d} e^{-jk_{x0}kd} = B_{k'} M_{k'}(x)\, cot(k_0 h_{k'})\, e^{-jk_{x0}k'd} \tag{14}$$

where $k' = 1, 2, 3, \ldots m$

From (14), we can build a $m \times m$ matrix M. Then, the amplitude coefficients $B = (B_1, B_2, \ldots, B_m)^T$ can be solved by linear matrix equation $MB = 0$, where

$$M(k', k) = S_{k'-k} - \delta_{k'k} T_k$$

$$S_{k'-k} = \sum_{n=-\infty}^{\infty} j\frac{k_0}{k_{zn}} \left(\frac{a}{p}\right) Sa^2\left(\frac{k_{xn}a}{2}\right) e^{jk_{xn}(k-k')d}$$

$$T_k = cot(k_0 h_k)\, e^{-jk_{x0}kd}$$

Finally, in order to ensure the coefficients matrix B has nonzero solution, and the determinant of the matrix M is set 0. In this way, the dispersion equation of the super-grating is obtained as:

$$|M| = 0 \tag{15}$$

APPENDIX B

Relation between the radiation direction, frequency and the energy of the free electron.

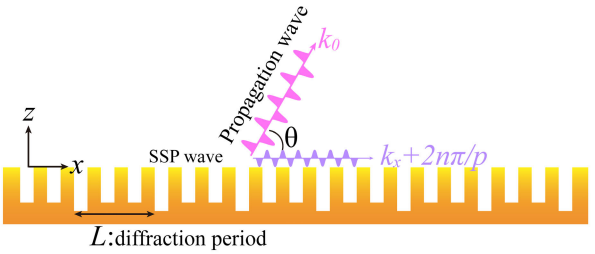

FIGURE 5. The diffraction relation between the wavenumber of SSP wave and a propagation wave.

As the 0-th wavenumber k_{x0} of SSP is far larger than that of the wave vector k_0 in free space, it cannot be converted to spatial radiation directly. Yet the negative harmonic wave whose wavenumber k_{x0} is smaller than k_0 can be coupled out as a propagation wave as shown in the Fig. 5. Assuming that the angle between the propagation wave and the x axis is θ, the relation between the n-th harmonic wave and a propagation wave is illustrated as (16) based on the diffraction theory,

$$k_{x0} - \frac{2\pi}{L}|n| = k_0 cos\theta \tag{16}$$

where L is the diffraction period, n is a negative integer, At the operating frequency,

$$k_{x0} = \frac{\omega}{v_e} \tag{17a}$$

$$k_0 = \frac{\omega}{c} \tag{17b}$$

Substitutes (17) into (16), it yields,

$$\frac{c}{f} = \frac{L}{|n|}\left(\frac{c}{v_e} - cos\theta\right) \tag{18}$$

ACKNOWLEDGMENT

The authors would like to thank Dr. Bao-Liang Hao, Beijing Vacuum Electronics Research Institute, China, for his support for the CST software simulation.

REFERENCES

[1] P. H. Siegel, "Terahertz technology," *IEEE Trans. Microw. Theory Techn.*, vol. 50, no. 3, pp. 910–928, Mar. 2002.
[2] M. Tonouchi, "Cutting-edge terahertz technology," *Nature Photon.*, vol. 1, no. 2, pp. 97–105, Feb. 2007.
[3] P. H. Siegel, "Terahertz technology in biology and medicine," *IEEE Trans. Microw. Theory Techn.*, vol. 52, no. 10, pp. 2438–2447, Oct. 2004.
[4] J. A. Fülöp, L. Pálfalvi, G. Almási, and J. Hebling, "Design of high-energy terahertz sources based on optical rectification," *Opt. Express*, vol. 18, no. 12, pp. 12311–12327, May 2010.

[5] M. M. Assefzadeh and A. Babakhani, "Broadband oscillator-free THz pulse generation and radiation based on direct digital-to-impulse architecture," *IEEE J. Solid-State Circuits*, vol. 52, no. 11, pp. 2905–2919, Nov. 2017.
[6] M. Y. Glyavin, A. G. Luchinin, and G. Y. Golubiatnikov, "Generation of 1.5-kW, 1-THz coherent radiation from a gyrotron with a pulsed magnetic field," *Phys. Rev. Lett.*, vol. 100, no. 1, Jan. 2008, Art. no. 015101.
[7] J. C. Tucek, M. A. Basten, D. A. Gallagher, and K. E. Kreischer, "Operation of a compact 1.03 THz power amplifier," presented at the IVEC, 2016. [Online]. Available: https://ieeexplore.ieee.org/abstract/document/7561772
[8] H. Xi, J. Wang, Z. He, G. Zhu, Y. Wang, H. Wang, Z. Chen, R. Li, and L. Liu, "Continuous-wave Y-band planar BWO with wide tunable bandwidth," *Sci. Rep.*, vol. 8, no. 1, Jan. 2018, Art. no. 348.
[9] R. Li, C. Ruan, A. K. Fahad, C. Zhang, and S. Li, "Broadband and high-power terahertz radiation source based on extended interaction klystron," *Sci. Rep.*, vol. 9, no. 1, Mar. 2019, Art. no. 4584.
[10] J. B. Pendry, L. Martín-Moreno, and F. J. Garcia-Vidal, "Mimicking surface plasmons with structured surfaces," *Science*, vol. 305, no. 5685, pp. 847–848, Aug. 2004.
[11] Y. J. Guo, K. Da Xu, Y. Liu, and X. Tang, "Novel surface plasmon polariton waveguides with enhanced field confinement for microwave-frequency ultra-wideband bandpass filters," *IEEE Access*, vol. 6, pp. 10249–10256, 2018.
[12] S. Shen, B. Xue, M. Yu, and J. Xu, "A novel three-dimensional integrated spoof surface plasmon polaritons transmission line," *IEEE Access*, vol. 7, pp. 26900–26908, Dec. 2019.
[13] L.-B. Kong, C.-P. Huang, C.-H. Du, P.-K. Liu, and X.-G. Yin, "Enhancing spoof surface-plasmons with gradient metasurfaces," *Sci. Rep.*, vol. 5, Mar. 2015, Art. no. 8772.
[14] Y.-Q. Liu, C.-H. Du, and P.-K. Liu, "Terahertz electronic source based on spoof surface plasmons on the doubly corrugated metallic waveguide," *IEEE Trans. Plasma Sci.*, vol. 44, no. 12, pp. 3288–3294, Mar. 2016.
[15] J.-F. Zhu, C.-H. Du, L.-Y. Bao, and P.-K. Liu, "Regenerated amplification of terahertz spoof surface plasmon radiation," *New J. Phys.*, vol. 21, Mar. 2019, Art. no. 033021.
[16] Y. Zhang, Y. Zhou, Y. Gang, G. Jiang, and Z. Yang, "Coherent Terahertz Radiation from Multiple Electron Beams Excitation within a Plasmonic Crystal-like structure," *Sci. Rep.*, vol. 7, Jan. 2017, Art. no. 41116.
[17] H.-H. Tang, T.-J. Ma, and P.-K. Liu, "Experimental demonstration of ultra-wideband and high-efficiency terahertz spoof surface plasmon polaritons coupler," *Appl. Phys. Lett.*, vol. 108, no. 19, May 2016, Art. no. 191903.
[18] W. Sun, Q. He, S. Sun, and L. Zhou, "High-efficiency surface plasmon meta-couplers: Concept and microwave-regime realizations," *Light-Sci. Appl.*, vol. 5, no. 1, Jan. 2016, Art. no. e16003.
[19] A. Okajima and T. Matsui, "Electron-beam induced terahertz radiation from graded metallic grating," *Opt. Express*, vol. 22, no. 14, pp. 17490–17496, Jul. 2014.
[20] S. J. Smith and E. M. Purcell, "Visible light from localized surface charges moving across a grating," *Phys. Rev.*, vol. 92, p. 1069, Nov. 1953.
[21] I. Shih, D. B. Chang, J. E. Drummond, K. L. Dubbs, D. L. Masters, R. M. Prohaska, and W. W. Salisbury, "Experimental investigation of radiation from the interaction of an electron beam and a conducting grating," *Opt. Lett.*, vol. 15, no. 10, pp. 559–561, May 1990.
[22] A. Massuda, C. Roques-Carmes, Y. Yang, S. E. Kooi, Y. Yang, C. Murdia, K. K. Berggren, I. Kaminer, and M. Soljačić, "Smith–Purcell radiation from low-energy electrons," *ACS Photon.*, vol. 5, no. 9, pp. 3513–3518, Aug. 2018.
[23] S. Kim, I.-K. Baek, R. Bhattacharya, D. Hong, M. Sattorov, A. Bera, J.-K. So, D.-S. Kim, and G.-S. Park, "High-Q metallic Fano metamaterial for highly efficient cerenkov lasing," *Adv. Opt. Mater.*, vol. 6, no. 12, Apr. 2018, Art. no. 1800041.
[24] E. M. Khutoryan, Y. S. Kovshov, A. S. Likhachev, S. S. Ponomarenko, S. A. Kishko, K. A. Lukin, V. V. Zavertanniy, T. V. Kudinova, S. A. Vlasenko, A. N. Kuleshov, and T. Idehara, "Excitation of hybrid space-surface waves in clinotrons with non-uniform grating," *J. Infr., Millim., THz. Waves*, vol. 39, no. 3, pp. 236–249, Nov. 2017.
[25] K. Zhang, D. Li, K. Chang, K. Zhang, and D. Li, *Electromagnetic Theory for Microwaves and Optoelectronics*. Springer, 1998, ch. 7, secs. 4–7, p. 404.
[26] Z. L. Deng, N. Yogesh, X. D. Chen, W. J. Chen, J. W. Dong, Z. Ouyang, and G. P. Wang, "Full controlling of Fano resonances in metal-slit superlattice," *Sci. Rep.*, vol. 5, Dec. 2015, Art. no. 18461.
[27] A. P. Hibbins, J. R. Sambles, and C. R. Lawrence, "Excitation of remarkably nondispersive surface plasmons on a nondiffracting, dual-pitch metal grating," *Appl. Phys. Lett.*, vol. 80, no. 13, pp. 2410–2412, Feb. 2012.
[28] CST Corporation. *CST PS Tutorials*. [Online]. Available: https://www.cst.com
[29] W. Liu and Z. Xu, "Special Smith–Purcell radiation from an open resonator array," *New J. Phys.*, vol. 16, Jul. 2014, Art. no. 073006.

JUAN-FENG ZHU received the B.E. degree in electronic information science and technology from Lanzhou University, Lanzhou, China, in 2016. He is currently pursuing the Ph.D. degree with the Department of Electronics, Peking University, Beijing, China.

His current research interests include millimeter–terahertz electronic devices and their applications.

CHAO-HAI DU (SM'16) received the B.S. degree in electronics from the University of Electronic Science and Technology of China, Chengdu, China, in 2005, and the Ph.D. degree in physical electronics from the University of Chinese Academy of Sciences, Beijing, China, in 2010.

He is currently a Research Professor with Peking University, Beijing.

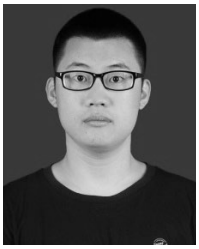

FAN-HONG LI received the B.E. degree in electromagnetic field and wireless technology from Northwestern Polytechnical University, Xi'an, China, in 2018. He is currently pursuing the Ph.D. degree with the Department of Electronics, Peking University, Beijing, China.

His research interests include terahertz electronic devices and their applications.

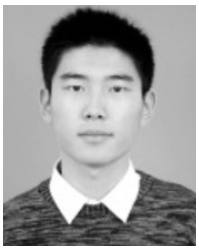

LU-YAO BAO received the B.E. degree in nuclear science and technology from the University of Science and Technology of China, Hefei, China, in 2017. He is currently pursuing the M.S. degree with the Department of Electronics, Peking University, Beijing, China.

His research interests include terahertz electronic devices and their applications.

PU-KUN LIU (SM'02) received the Ph.D. degree in nuclear fusion and plasma physics from the Southwestern Institute of Physics, Chengdu, China, in 1995.

From 1996 to 1998, he was a Postdoctoral Researcher with Peking University, Beijing, China, and with Tel Aviv University, Tel Aviv, Israel. From 1999 to 2000, he was an Alexander-von-Humboldt Research Fellow with Forschungszentrum Karlsruhe, Karlsruhe, Germany. From 2000 to 2013, he was a Research Professor with the Institute of Electronics, Chinese Academy of Sciences, Beijing. Since 2013, he has been a Full Professor (Tenure) with the Department of Electronics, Peking University.